Talanta 103 (2013) 194–200

Contents lists available at SciVerse ScienceDirect

Talanta

journal homepage: www.elsevier.com/locate/talanta

Interaction of ciprofloxacin with DNA studied by spectroscopy and voltammetry at MWCNT/DNA modified glassy carbon electrode

Lida Fotouhi *, Zeynab Atoofi, Majid M. Heravi

Alzahra University, Department of Chemistry, School of Science, Vanak, Tehran 1993891167, Iran

ARTICLE INFO

Article history:
Received 3 July 2012
Received in revised form
6 October 2012
Accepted 8 October 2012
Available online 17 October 2012

Keywords:
Ciprofloxacin
DNA
Multi-walled carbon nanotubes (MWCNT)
Cyclic voltammetry
Binding constant
Fluorescence

ABSTRACT

The interaction of ciprofloxacin (Cf) with double-stranded DNA was studied by cyclic voltammetry, fluorescence emission spectroscopy, and UV–Vis spectroscopy. The presence of DNA results in a decrease in the current and a positive shift in the Cf oxidation peak indicates the intercalative interaction. The corresponding heterogeneous rate constant (k_s) and the electron transfer coefficient (α) were calculated for free Cf and the bound Cf–DNA complex. The UV spectroscopic data confirmed the interaction between Cf and DNA is intercalative. Besides, the fluorescence emitted by Cf at 420 nm could be quenched in Britton–Robinson (B–R) buffer solution (pH 7.0, 0.04 mol L^{-1}) when DNA was added. The mechanism of fluorescence quenching was a static quenching; the binding constant and numbers of binding sites were obtained from the Stern–Volmer plot. The calibration curve was found to be linear between F_0/F and the DNA concentration is lied in the two dynamic ranges of 0.8–96.0 and 96.0–223 μg mL^{-1} with the detection limit of 0.33 μg mL^{-1}. The method was efficaciously applied to analyze DNA in the serum sample.

1. Introduction

Quinolones are an interesting group of antibacterials. The mechanism of action of these compounds is inhibition of DNA gyrase and DNA topoisomerase IV that control DNA topology and are vital for bacterial replication [1]. Almost all the recent clinically useful quinolones bear a fluorine atom in the C-6 position and thus these antibacterial agents are called fluoroquinolones. Ciprofloxacin (Cf) belongs to second-generation fluoroquinolones and is used in a wide range of gastrointestinal, urinary, and respiratory tract, ocular, and skin infections along with patients with intra-abdominal infections in combination with antianaerobic agents [2].

DNA as a molecule of great biological significance carries genetic information in a cell. It is the major target for drug interaction as it is the outset of the most important cellular processes of storage, copying, and transmission of gene messages. Small ligand molecules bound upon DNA which are artificially modulate inhibit the DNA functioning. Therefore, the studies on the binding nature of these small molecules upon DNA are very interesting not only in understanding the mechanism of interaction, but also for guiding the design of new drugs [3,4].

Alternatively, carbon nanotubes (CNTs) have drawn much attention in recent years as a new class of conducting materials for use in biomaterial fabrication because of their unique structure, high chemical stability, surface-to-volume ratio and excellent electrical and mechanical properties [5].

Drug-DNA interactions have been studied by a variety of analytical methods such as luminescence [6], UV–vis [7], fluorescence [8], FT-IR [9], NMR [10], and electroanalytical methods [11–12]. Among these methods, voltammetry and fluorescence are very common ones. Voltammetric studies of the interaction of berberin with DNA immobilized on glassy carbon electrode (GCE) have been reported [13]. The interaction of DNA with curcumin in the presence of Cu(II) has been investigated by differential pulse adsorptive transfer voltammetry [14]. Ulrih et al. [15] investigated Mg^{+2} and Cu^{+2}-mediated Cf binding to the linear genomic DNA at pH 7.0, by fluorescence and UV spectroscopy. Khalid et al. [16] studied the interaction of Cf with DNA using an electrochemical DNA biosensor, which was immobilized on bare GCE. They used the guanine oxidation peak as gauge for the maximum surface coverage of the GCE by constant current potentiometry and differential pulse voltammetry which showed that Cf binds to DNA in two different modes: electrostatic and intercalative. However, the research interest in biomaterial-assisted fabrications of various nanostructures keeps growing over the past years. Deng et al. [17] has reported a DNA-assisted electrode deposition of palladium nanoparticles on GCE. Nevertheless, to the best of our knowledge, little is identified about the kinetic parameters of

* Corresponding author. Tel.: +98 218 804 4040; fax: +98 218 803 5187.
E-mail addresses: lida_fotouhi@yahoo.com, lfotouhi@alzahra.ac.ir (L. Fotouhi).

0039-9140/$ - see front matter © 2012 Elsevier B.V. All rights reserved.
http://dx.doi.org/10.1016/j.talanta.2012.10.032

Cf and its interaction with DNA on an MWCNT modified GCE. Following our recent studies [18–20], in this article the interaction of Cf with DNA immobilized on a MWCNT modified GCE has been studied by cyclic voltammetry. Furthermore, interaction of Cf with DNA has also been investigated by fluorescence spectroscopy and UV spectroscopy. An additional procedure for determination of DNA in serum via intrinsic fluorescence quenching of Cf with DNA has been developed.

2. Experimental

2.1. Apparatus

Electrochemical measurements were carried out with a Metrohm model 746 VA trace analyzer connected to a 747 VA stand. The working electrode was a glassy carbon electrode (2 mm diameter). A platinum wire and a commercial Ag/AgCl saturated KCl electrode from Metrohm were used as auxiliary and reference electrodes, respectively. All the electrochemical measurements were carried out in a 10 mL electrolytic cell.

Absorption spectra were measured on a UV–vis spectrophotometer Lambda 35-Perkin Elmer. Fluorescence emission spectra were measured using a 1 cm path length quartz cuvette and a Varian Cary Eclipse Model fluorescence spectrophotometer equipped with a water thermostated cell holder.

The pH measurements were carried out with a Metrohm Model 744 pH meter.

2.2. Chemicals

Double-stranded calf thymus DNA was purchased from Sigma. Ciprofloxacin was obtained from Aldrich. Multi-walled carbon nanotubes with purity 95% (10–30 nm diameters and 5 μm length) were obtained from io-li-tec, Ionic Liquid Technologies. All other reagents used were of analytical grade. All aqueous solutions were prepared in doubly distilled, deionized water.

2.3. General procedures

All of the electrochemical, UV–vis and fluorescence measurements were made in B–R buffer solution (pH 7.0, 0.04 mol L^{-1}).

2.3.1. Stock solutions

A stock Britton–Robinson (B–R) buffer solution 0.04 mol L^{-1} with respect to boric acid, orthophosphoric acid and acetic acid were prepared from proanalysis reagents. From this stock buffer, solutions with various values of pHs were prepared by the addition of 1.0 mol L^{-1} sodium hydroxide solution. The stock solution of DNA (10^3 μg mL^{-1}) was prepared in B–R buffer solution (pH 7.0, 0.04 mol L^{-1}) and stored at 4 °C. Dilution was done just prior to use. The concentration of DNA was calculated according to the absorbance at 260 nm by using $\varepsilon_{DNA}=6600$ mol^{-1} L cm^{-1} [21].

2.3.2. Electroanalytical procedure

For electrochemical measurements 4.0 mL of 2.0 mmol L^{-1} stock solution of Cf were placed into the cell to make up 10.0 mL solution at a Cf concentration of 0.8 mmol L^{-1}. The voltammograms were recorded with cyclic potential range between 600 to 1000 mV. All electrochemical experiments were carried out at room temperature.

2.3.2.1. Preparation of the MWCNT and MWCNT/DNA hybrid composites. MWCNT (4.0 mg) was added to 1.0 mL DMF. A homogeneous and stable suspension of 4.0 mg mL^{-1} MWCNT was achieved with the aid of ultrasonic agitation for about 30 min. Then 20 μL of the black suspension of MWCNT was added to the 20 μL of 400 μg mL^{-1} DNA and the resulting suspension was kept in an ice–water bath and sonicated for 60 s. A homogeneous well-distributed suspension of MWCNT/DNA hybride composite then obtained.

2.3.2.2. Fabrication of MWCNT/GCE and MWCNT/DNA/GCE. Prior to the immobilization, glassy carbon electrode was sanded using ultrafine sand paper, polished with 10 μm alumina slurry in sequence and sonicated in water for 10 min. The MWCNT/GCE was prepared by casting 3.0 μL of the suspension of MWCNT on the surface of a GCE, which was dried in air for 30 min at room temperature. The immobilization of DNA was performed by casting the GCE with 6.0 μL of the MWCNT/DNA hybrid composite and allowed to dry in air for 30 min at room temperature. The resulting electrode is called MWCNT/DNA/GCE.

2.3.3. Fluorescence emission spectroscopy

The emission spectra were recorded in the range of 280–550 nm at an excitation wavelength of 272 nm. Fluorescence titration profiles were determined by incrementally adding aliquots of DNA into a cuvette containing a known amount of Cf (14 μmol L^{-1}). The emission spectra of Cf, corrected for the solvent blank were multiplied by the dilution factor and subtracted from the fluorescence spectrum of Cf in B–R buffer solution (0.04 mol L^{-1}, pH 7.0).

2.3.4. UV spectroscopy

The absorption spectrum of a known concentration of Cf was obtained without DNA. The spectroscopic response of the same amount of Cf was then monitored by the addition of small aliquots of DNA solution.

3. Results and discussion

3.1. Voltammetric studies of Cf-DNA interaction

Fig. 1A compares the cyclic voltammograms of Cf in B–R buffer solution (0.04 mol L^{-1}, pH 7.0) at MWCNT/GCE and MWCNT/DNA/GCE. As shown in Fig. 1A, curve a, the Cf has an irreversible anodic peak current of 18.6 μA at 0.922 V, which is related to the electrode oxidation of the amine group to hydroxylamine. According to our previous work [20], MWCNT exhibited excellent electrocatalytic behavior in the oxidation of Cf as evidenced by enhancement of the Cf oxidation peak current and shift in the Cf oxidation potential to lower values (by 130 mV) in comparison with the bare GCE. In the presence of DNA, a decrease in the Cf oxidation peak current and a positive shift in the Cf oxidation peak were observed (Fig. 1A, curve b), which indicates the interaction of Cf with DNA. The diminution of oxidation peak current is attributed to decrease of the free drug concentration due to formation of slowly diffusing Cf-DNA complex. Here, with the addition of DNA, the oxidation peak potential is shifted to a more positive potential, from 0.922 to 0.947, which suggestd that the Cf interaction with DNA is intercalation [22–24]. As can be seen from Fig. 1B, in the absence of Cf, no redox peaks was observed at both MWCNT/GCE (curve a) and MWCNT/DNA/GCE (curve b) during the cyclic voltammetry within the potential window from 0.6 to 1.0 V.

Useful information about the interaction of drugs and biomolecules usually can be acquired from the cyclic voltammetry that is one of the most important electroanalytical techniques due to the similarity among various redox chemical and biological processes [25]. Since binding of Cf to DNA may influence the major electrochemical kinetic parameters of Cf (such as α and k_s) the cyclic voltammograms of Cf at various scan rates were

recorded on the surface of both MWCNT/DNA/GCE (bound Cf-DNA) and MWCNT/GCE (free Cf). Fig. 2A shows the typical cyclic voltammograms of Cf at various scan rates on the MWCNT/DNA/GCE. An linear relationship between the peak current and the scan rate revealed Cf oxidation was an adsorption-controlled process (Fig. 2B). Furthermore, from the slopes of the linear plots of I vs. υ the surface concentrations of electroactive species (Γ) were estimated as 3.13×10^{-6} and 2.93×10^{-6} mol cm^{-2} for the free Cf and the bound Cf–DNA, respectively, according to the following equation [26]:

$$I = n^2F^2A\Gamma\upsilon/4RT \quad (1)$$

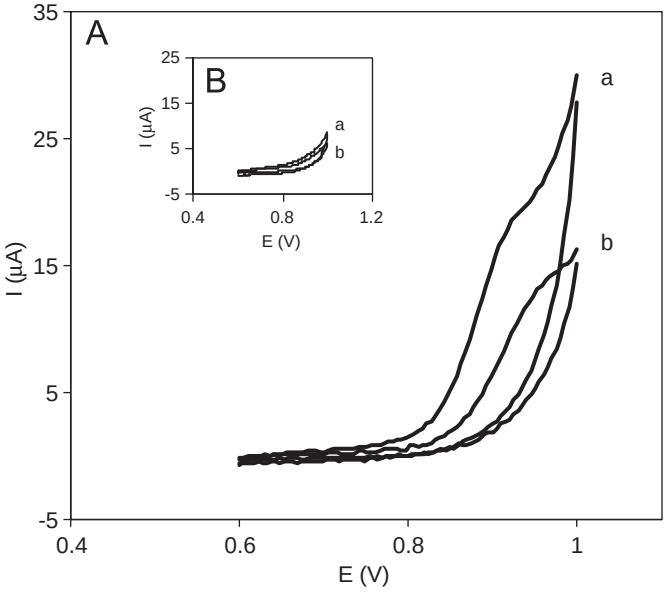

Fig. 1. (A) Cyclic voltammograms of (a) 0.8 mmol L^{-1} Cf at MWCNT/GCE, (b) 0.8 mmol L^{-1} Cf at MWCNT/DNA/GCE. (B) Cyclic voltammograms of blank solution at (a) MWCNT/GCE, (b) MWCNT/DNA/GCE, in B–R buffer (pH 7.0, 0.04 mol L^{-1}) scan rate: 50 mV s^{-1}.

where n represents the number of electrons involved in reaction (two electrons), A is the surface area (0.03 cm^2) of the GCE, T is temprature (25 °C), Γ (mol cm^{-2}) is the surface coveraged and other symbols have their usual meaning.

As it is shown by increasing the scan rate, the peak potential shifted to a more positive potential. For a totally irreversible and an adsorption-controlled process, the relationship between E_P and υ can be expressed by the Laviron's equation [27]:

$$E_p = E^0 - 2.3RT/\alpha nF[\log(RTk_s/\alpha nF) - \log\upsilon] \quad (2)$$

where E^0 (V) was the formal potential, α was the transfer coefficient, k_s (s^{-1}) was the electrochemical rate constant and other symbols have their usual meaning. k_s and αn values can be obtained from the intercept and the slope of the linear plot of E_p with respect to log υ, if the E^0 is known.

The E^0 value can be deduced from the intercept of E_p vs. υ plot on the ordinate by extrapolating the line to $\upsilon = 0$ V s^{-1}. By knowing E^0 and graphical representations of E_p vs. log υ for Cf in the absence and presence of DNA (Fig. 2D), the αn and k_s values were obtained from the slope and intercept, respectively (Table 1). On the assumption that the number of electrons involved in the Cf oxidation is 2 the values of α for an irreversible surface reaction can be obtained as 0.43 and 0.39 for the free Cf (at MWCNT/GCE) and the bound Cf-DNA (at MWCNT/DNA/GCE), respectively. As shown by the data obtained, the value of α decreased while the value of k_s decreased in the presence of DNA. Decreasing of α may be due to higher absorption of Cf-DNA complex at the electrode surface while decreasing of k_s may be

Table 1
The electrochemical parameters calculated from the results of cyclic voltammetry.

Electrode	k_s (s^{-1})	αn	Γ (mol cm^{-2})
MWCNT/GCE	0.298	0.856	3.13×10^{-6}
MWCNT/DNA/GCE	0.227	0.780	2.93×10^{-6}

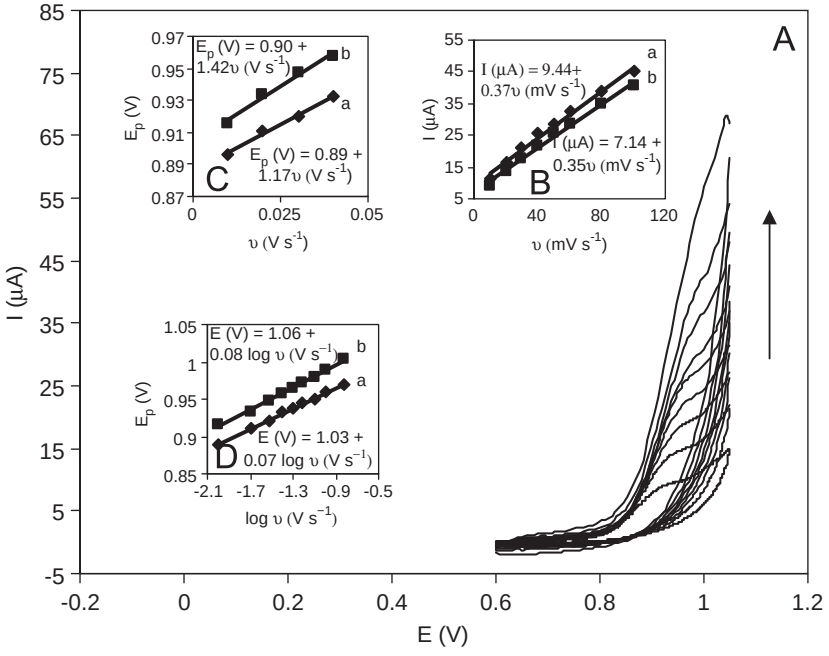

Fig. 2. (A) Cyclic voltammograms of 0.8 mmol L^{-1} Cf at MWCNT/DNA/GCE in B–R buffer (pH 7.0, 0.04 mol L^{-1}) at scan rates (inner to outer) 10, 20, 30, 40, 50, 60, 80, 100, and 150 mV s^{-1}. (B) The plots of peak currents vs. scan rate for the free Cf (at MWCNT/GCE) (a) and the bound Cf-DNA (at MWCNT/DNA/GCE) (b). ((C) and (D)) The variations of peak potential vs. υ and log υ for the free Cf (a) and the bound Cf–DNA (b), respectively.

attributed to the lower rate of electron transfer of Cf in the form of Cf-DNA supracomplex.

Both the oxidation peak current and peak potential were dependent upon the pH of the buffer solution. By increasing the pH from 2.0 to 10, the Cf oxidation peak shifts to less positive potentials. Fig. 3 shows two defined breaks corresponding to the apparently pK_a values, 6.0 and 7.3. The pK_a values are in excellent agreement with literature [28]. According to the fitting line in the pH ranges of 2.0 to 6.0 (E_p(V)=1.40−0.055 pH), the ratio of proton to electron 0.93 is obtained, which can be accepted as one suggesting that the number of the electrons transferred in the Cf oxidation at MWCNT/DNA/GCE is equal to that of protons.

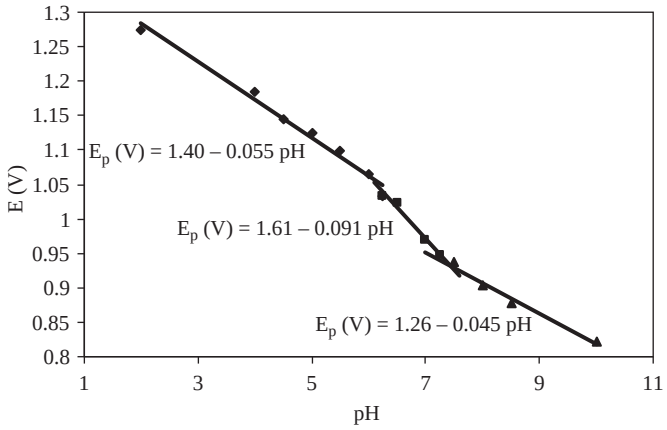

Fig. 3. linear plot of E vs. pH at MWCNT/DNA/GCE for pH values of (a) 2.0, (b) 4.0, (c) 4.5, (d) 5.0, (e) 5.5, (f) 6.0, (g) 6.5, (h) 7.0, (i) 7.5, (j) 8.0, and (k) 10.0 in B–R buffer (0.04 mol L^{-1}), scan rate 50 mV s^{-1}.

3.2. Determination of binding constant of Cf to DNA

In this section, the binding behavior of Cf to MWCNT/DNA/GCE was measured by recording the cyclic voltammograms of Cf at various concentrations (Fig. 4A). As is obvious, the peak current increased by increase in the Cf concentration (C_{Cf}) and then trended to saturation values (Fig. 4B), as expected with the shape of Langmuir adsorption. Thus the adsorption thermodynamics follows equation [29]:

$$C_{Cf}/I = (1/KI\max) + (C_{Cf}/I_{max}) \quad (3)$$

where I, I_{max}, C_{Cf} and K are the peak current, maximum peak current, Cf concentration, and the binding constant of Cf to DNA at MWCNT/DNA/GCE surface. Fig. 4C shows the plot of C_{Cf}/I vs. C_{Cf} at MWCNT/DNA/GCE. K value can be obtained from the linear regression equation as 2.39×10^3 mol^{-1} L.

3.3. UV spectroscopy for characterization of the interaction of Cf with DNA

The interaction of Cf with DNA was also investigated by UV–Vis absorption titration in the B-R buffer solution (pH 7.0, 0.04 mol L^{-1}) by maintaining the Cf concentration constant but changing the DNA concentration. An absorbance peak at 260 nm is shown by DNA in aqueous solution (data not shown). As shown in Fig. 5, Cf has two absorption wavelengths at 272 and 323 nm. With the addition of DNA into Cf solution, the absorption at 323 nm is decreased gradually (hypochromism), whereas the absorption at 272 nm is remarkably increased (hyperchromism). Appearance of isobestic point at 294 nm is due the intensive binding Cf with DNA and formation of new complex. Based on the above results, we suggested that the interaction mode between Cf and DNA is intercalative interaction, which is in agreement with the literature [30].

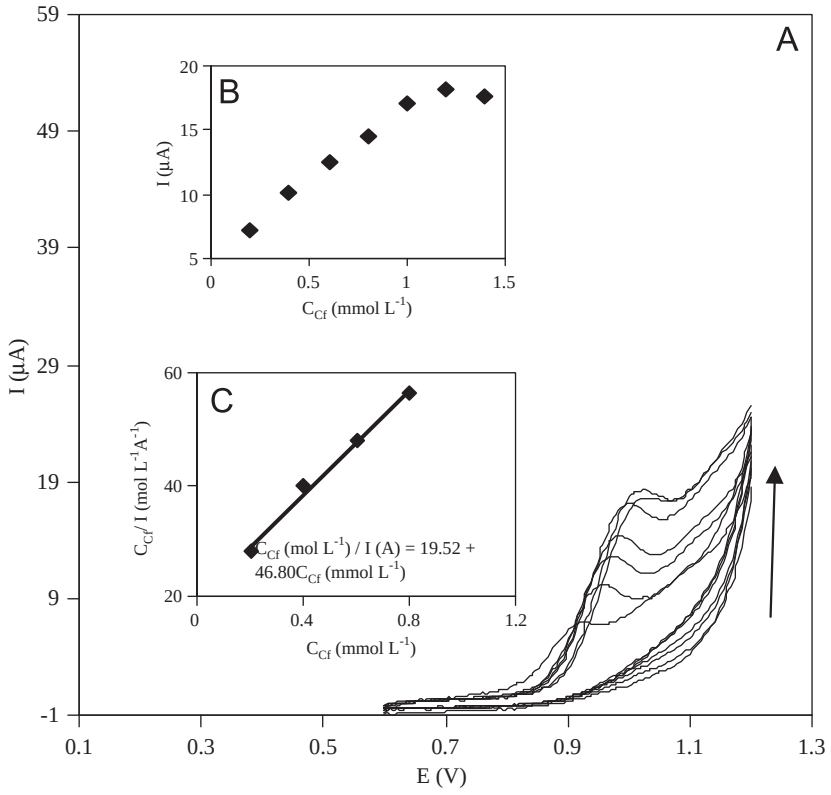

Fig. 4. (A) The cyclic voltammograms of Cf at various concentrations (inner to outer): 0.2, 0.4, 0.6, 0.8, 1.2, and 1.4 mmol L^{-1}. (B) The plot of I vs. C_{Cf}, (C) The linear plot of C_{Cf}/I vs. C_{Cf}.

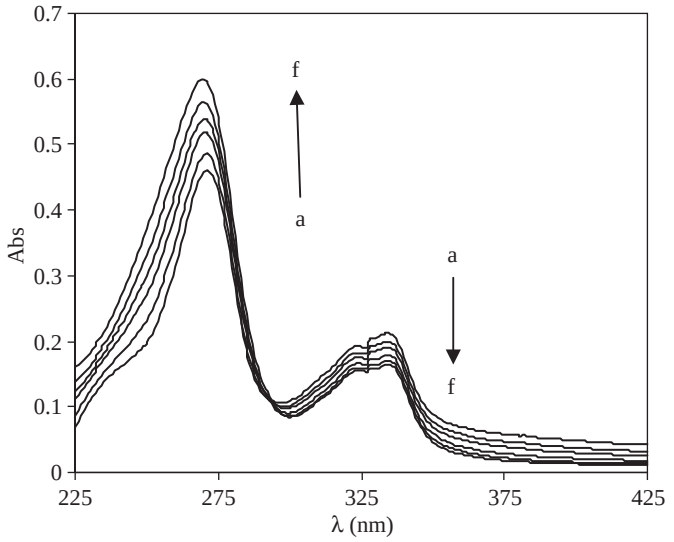

Fig. 5. The UV spectra of Cf and Cf–DNA complex in B–R buffer solution (0.04 mol L^{-1}, pH 7.0). Curve (a): 1.40×10^{-5} mol L^{-1} Cf; (b): (a)+0.44×10^{-5} mol L^{-1} DNA; curve (c): (a)+0.86×10^{-5} mol L^{-1} DNA; curve (d): (a)+1.12×10^{-5} mol L^{-1} DNA; curve (e): (a)+1.70×10^{-5} mol L^{-1} DNA; curve (f): (a)+2.12×10^{-5} mol L^{-1} DNA.

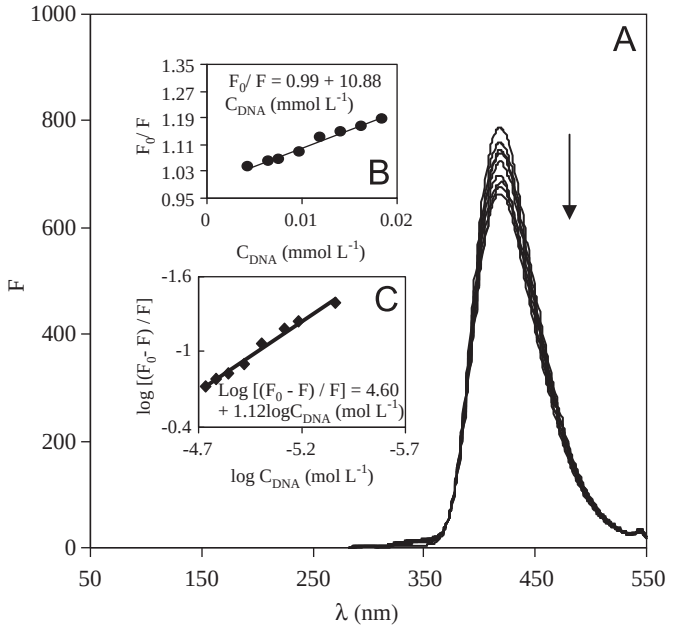

Fig. 6. (A) The fluorescence quenching spectra of 1.4×10^{-5} mol L^{-1} Cf; in B–R buffer (pH 7.0, 0.04 mol L^{-1}) in various concentration of DNA from up to down: 0, 0.44×10^{-5}, 0.66×10^{-5}, 0.76×10^{-5}, 0.98×10^{-5}, 1.20×10^{-5}, 1.42×10^{-5}, 1.64×10^{-5} and 1.86×10^{-5} mol L^{-1} DNA, (B) The linear plot of F_0/F vs. concentration of DNA, (C) The linear plot of $\log[(F_0-F)/F]$ vs. $\log C_{DNA}$.

3.4. Fluorescence spectroscopy

The interaction of Cf with DNA was also examined by fluorescence titration. Solution of free Cf displays intrinsic fluorescence with maximum excitation and emission wavelengths at 272 and 420 nm, respectively, whereas DNA has no fluorescence. Fig. 6A shows the fluorescence spectra of Cf in B–R buffer (pH 7.0, 0.04 mol L^{-1}) in the absence and presence of different DNA concentrations. It can be seen that addition of different concentrations of DNA to a fixed concentration of Cf (14 μmol L^{-1}) caused a decrease in the Cf fluorescence intensity, indicating the quenching of Cf fluorescence intensity upon binding to DNA.

Generally, fluorescence quenching includes several mechanisms such as dynamic quenching, static quenching, and the combined static and dynamic quenching. If the quenching mechanism belongs to the combined static and dynamic quenching, it follows the Stern–Volmer equation [31]:

$$F_0/F = 1+(K_D+K_S)[Q]+K_DK_S[Q]^2 \quad (4)$$

where K_D and K_S are the dynamic and the static quenching constants, respectively. F_0 and F are the fluorescence intensities in the absence and presence of quencher. $[Q]$ is the molar concentration of quencher (DNA). In this case, the Stern–Volmer plot is characterized by a non-linear behavior. As can be seen in the plot F_0/F vs. C_{DNA} (Fig. 6B), the quenching mechanism was not combined static and dynamic quenching due to the linearity of the Stern–Volmer plot.

The linear relationship between the Cf fluorescence and DNA concentration can be used to determine the type of quenching, static or dynamic by the classical Stern–Volmer relationship [31]:

$$F_0/F = 1+k_q\tau_0[Q] = 1+K_{SV}[Q] \quad (5)$$

Generally, the fluorescence lifetime (τ_0) of biological macromolecule is approximately 10^{-8} s. Thus, the quenching constant k_q can be calculated from the slope of the linear Stern–Volmer plot (Fig. 6B), ($F_0/F=0.99+10.90$ C_{DNA} (mmol L^{-1})) as 108.8×10^{10} mol^{-1} L s^{-1}, which is much larger than the limiting diffusion control collision constant of biomolecule (2.0×10^{10} mol^{-1} L s^{-1}). Thus, the quenching type of Cf by DNA should be static quenching rather than dynamic quenching.

The binding constant K_b and the binding sites n, when small molecules bind independently to a set of equivalent sites on a macromolecule, can be calculated using the following equation [32]:

$$\log[(F_0-F)/F] = \log K_b + n\log[\mathrm{DNA}] \quad (6)$$

K_b and n was obtained from double-logarithm linear curve of $\log[(F_0-F)/F]$ vs. $\log C_{DNA}$ as 3.98×10^4 mol^{-1} L and 1.12, respectively (Fig. 6C).

3.5. Optimization of variables for DNA determination

The effect of pH on the Cf fluorescence and its complex with DNA was examined, and the results showed that the fluorescence intensity was not affected by the changes in pH.

The effect of ionic strength was also determined by adding NaCl to the Cf solution, to which DNA was added subsequently to quench the Cf fluorescence. The experimental results confirmed that the Cf fluorescence intensity remained constant and has not any influence on the results.

Under the optimum conditions, the interferences of various foreign ions and other possibly coexisting substance in the fluorescence quenching by DNA were studied when the concentration of DNA wad 3.0 μg mL^{-1}. The results were shown as follow: the tolerance of NO_3^- was 480.0 μg mL^{-1}, the tolerance of K^+ and Cl^- was 320.0 μg mL^{-1}. The tolerance of Al^{3+}, Sr^{2+}, Cu^{2+}, SO_4^{2-}, and CO_3^{2-} was 160.0 μg mL^{-1}, and the tolerance of Ba^{2+}, lysine, glutamic acid, arginine, cysteine, and threonine was 60.0 μg mL^{-1}. It was found that this method had relatively high tolerance limits. Thus, small amounts of the foreign substances did not disturb the determination of DNA.

3.6. Calibration graph, reproducibility and detection limit

Under the optimized conditions mentioned above, calibration curves were obtained by plotting the F_0/F against the concentration of DNA (Fig. 7). The limits of detection (LOD) was given by 3 S_0/S, where 3 was the factor with 99% confidence level, S_0 was standard deviation of the blank measurements ($n=11$), and S was the

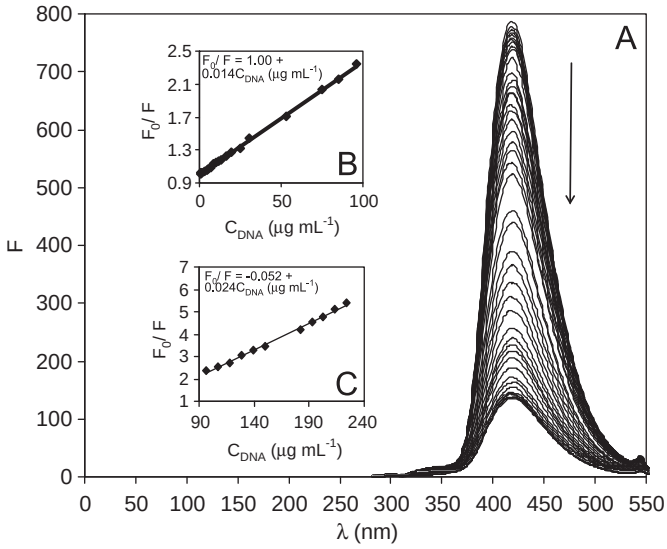

Fig. 7. (A) Fluorescence emission spectra of 1.4×10^{-5} mol L^{-1} Cf in B–R buffer (0.04 mol L^{-1}, pH 7.0) with various concentrations of DNA, C_{DNA}, (μg mL^{-1}) from up to down: 0, 0.8, 1.2, 1.6, 3.2, 4.8, 5.6, 7.2, 8.8, 10.4, 12.0, 13.5, 16.6, 19.8, 25.3, 30.8, 41.8, 52.8, 63.8, 74.6, 85.5, 96.0, 107.16, 118.0, 128.6, 139.3, 150.0, 181.8, 192.3, 202.8, 213.3, 223.0, 234.2, 244.6 and 254.5. ((B) and (C)) The plots of the F_0/F vs. C_{DNA}.

Table 2
Analytical figures of merit.

Parameter	
Calibration equation	$F_0/F=1.00+0.014\ C_{DNA}$ (μg mL^{-1}) $F_0/F=-0.052+0.024\ C_{DNA}$ (μg mL^{-1})
Linear dynamic range (μg mL^{-1})	0.8–96.0 and 96.0–223
Correlation coefficient	0.999 and 0.996
Detection limit (μg mL^{-1})	0.33
Quantification limit (μg mL^{-1})	1.11
R.S.D. (%) ($n=11$)	0.23

Table 3
Results of analysis of real samples.

Sample	Added (μg mL^{-1})	Found (μg mL^{-1})	Recovery (%)	R.S.D. (%) ($n=3$)
1	3.19	3.07	96	12.30
2	49.90	51.40	103	0.86
3	90.30	91.70	101	0.73

sensitivity of the calibration curve [33]. The lower limit linear range was set as the limit of quantitation (LOQ), which was given as 10 S_0/S [33]. Reproducibility and Relative standard deviation (R.S.D.) of the method were checked by successive determinations ($n=11$). Analytical parameters for the determination of DNA are shown in Table 2.

3.7. Application to real matrices

To evaluate the applicability of the present method on real matrices, assays were performed in the serum samples. To ascertain the validity of the results, the real samples were spiked with different amounts of DNA. The results showed that satisfactory recovery for DNA could be obtained (Table 3).

4. Conclusion

In this study, the interaction of Cf with DNA was investigated by voltammetric and spectroscopic methods. The voltammetric study revealed a marked decrease in anodic current of Cf with a positive shift in peak potential at the DNA modified electrode, which indicates the interaction of Cf with DNA. The electrochemical parameters of Cf in the absence and presence of DNA were calculated on the MWCNT/GCE. Khalid et al. [16] showed that Cf binds to DNA in two electrostatic and intercalative modes. However, our results showed that the intercalative binding of Cf is significant as compared with binding in the electrostatic in the presence of MWCNT. Detailed mechanism behind the influence of CNTs upon the interaction mode of the drugs with DNA is not clear at present. The bioconjugates of carbon nanotubes and DNA have potential applications in many areas due to the combination of the unusual structure of carbon nanomaterials and bioactivity of DNA reported in the literatures as below: The $\pi-\pi$ interactions between the nanotube sidewalls and nucleic acid bases [34], wrapping of CNTs in DNA, and attachment of oligonucleotides to the sidewalls of CNTs through hydrophobic interactions [35].

The UV spectroscopic data confirmed the interaction between Cf and DNA is intercalative. The fluorescence quenching mechanism between Cf and DNA was also studied. The results showed that a complex was formed between these species through static quenching interaction. The binding constant and binding sites were calculated as 3.98×10^4 mol^{-1} L and 1.12, respectively. In addition the change of the fluorescence is proportional to the amount of DNA added and the quantitative response has been applied to determination of DNA.

The combination of voltammetric and spectroscopic methods is of potential importance in understanding the mechanism of action of this important class of antibacterial agents and ultimately may be a useful guide to the design of more potent antibacterial agents with fewer side effects.

Acknowledgment

The authors gratefully acknowledge partial financial support from the Research Council of Alzahra University.

References

[1] E. Pestova, J.J. Millichap, G.A. Noskin, L.R. Peterson, Antimicrob. Agents Chemother. 45 (2000) 583–590.
[2] R. Davis, A. Markham, J.A. Balfour, Drugs 51 (1996) 1019–1074.
[3] X.H. Zhang, L.Y. Wang, Z.X. Nan, S.H. Tan, Z.X. Zhang, Dyes Pigm. 79 (2008) 205–209.
[4] K.L. Reddy, K.R.Y. Harish, K.K. Ashwini, S.S.S. Vidhisha, Nucleos. Nucleot. Nucl. 28 (2009) 204–219.
[5] V.N. Khabashesku, J.L. Margrave, E.V. Barrera, Diamond Relat. Mater. 14 (2005) 859–866.
[6] M.R. Arkin, E.D.A. Stemp, C. Turro, N.J. Turro, J.K. Barton, J. Am. Chem. Soc. 118 (1996) 2267–2274.
[7] C.Z. Huang, Y.F. Li, P. Feng, Talanta 55 (2001) 321–328.
[8] W. Zhong, J.H. Yu, Y. Liang, Spectrochim. Acta, Part A 59 (2003) 1281–1288.
[9] J.F. Neault, M. Naoui, M. Manfait, H.A. Tajmir-Riahi, FEBS Lett. 382 (1996) 26–30.
[10] T. Skauge, I. Turel, E. Sletten, Inorg. Chim. Acta 339 (2002) 239–247.
[11] Y.Q. Li, Y.J. Guo, X.F. Li, J.H. Pan, Talanta 71 (2007) 123–128.
[12] A.A. Ensafi, B. Rezaei, M. Amini, E. Heydari-Bafrooei, Talanta 88 (2012) 244–251.
[13] X. Tian, Y. Song, H. Dong, B. Ye, Bioelectrochemistry 73 (2008) 18–22.
[14] C. Serpi, Z. Stanić, S. Girousi, Talanta 81 (2010) 1731–1734.
[15] P. Drevensek, I. Turel, N.P. Ulrih, J. Inorg. Biochem. 96 (2003) 407–415.
[16] H. Nawaz, S. Rauf, K. Akhtar, A.M. Khalid, Anal. Biochem. 354 (2006) 28–34.
[17] C. Shao, N. Lu, Z. Deng, J. Electroanal. Chem. 629 (2009) 15–22.
[18] L. Fotouhi, S. Faramarzi, J. Electroanal. Chem. 568 (2004) 93–99.
[19] L. Fotouhi, F. Raei, M.M. Heravi, D. Nematollahi, J. Electroanal. Chem. 639 (2010) 15–20.
[20] L. Fotouhi, M. Allahyaei, Colloids Surf. B: Biointerfaces 81 (2010) 110–114.
[21] M.E. Reichman, S.A. Rice, C.A. Thomas, P.A. Doty, J. Am. Chem. Soc. 76 (1954) 3047–3053.
[22] Y. Wang, Y. Ni, S. Kokot, Anal. Biochem. 419 (2011) 76–80.
[23] Y. Wang, Y. Ni, S. Kokot, Chinese Chem. Lett. 21 (2010) 936–967.

[24] A. Shah, M. Zaheer, R. Qureshi, Z. Akhter, M.F. Naser, Spectrochim. Acta, Part A 75 (2010) 1082–1087.
[25] R.N. Goyal, A.B. Toth, G. Dryhurst, N.T. Nguyen, Bioelectrochem. Bioenerg. 9 (1982) 39–60.
[26] M. Shap, M. Petersson, K. Edstrom, J. Electroanal. Chem. 95 (1979) 123–130.
[27] E. Laviron, Electroanal. Chem. 101 (1979) 19–28.
[28] M.D. Prat, J. Benito, R. Compañó, J.A. Hernández-Arteseros, M. Granados, J. Chromatogr. A 1041 (2004) 27–33.
[29] X. Ju, Y.K. Ye, Y.L. Zhu, Electrochim. Acta 50 (2005) 1361–1367.
[30] Y.Q. Li, Y.J. Guo, X.F. Li, J.H. Pan, Talanta 71 (2007) 123–128.
[31] J.R. Lakowicz, Principles of Fluorescence Spectroscopy, second ed., Plenum Press, New York, 1986.
[32] X.Z. Feng, Zh. Lin, L.J. Yang, Ch. Wang, Ch.l. Bai, Talanta 47 (1998) 1223–1229.
[33] H.M.N.H. Irving, H. Freiser, T.S. West (Eds.), IUPAC Compendium of Analytical Nomenclature, Definitive Rules, Pergamon Press, Oxford, 1981.
[34] N. Nakashima, S. Okuzono, H. Marakami, T. Nakai, K. Yoshikawa, Chem. Lett. 32 (2003) 456–457.
[35] S. Danial, T.P. Rao, K.S. Rao, S.U. Rani, G.R.K. Naidu, H.Y. Lee, T. Kawai, Sens. Actuators, B: Chem. 122 (2007) 672–682.